iScience

CellPress

Article

The Reconfigurable Maze Provides Flexible, Scalable, Reproducible, and Repeatable Tests

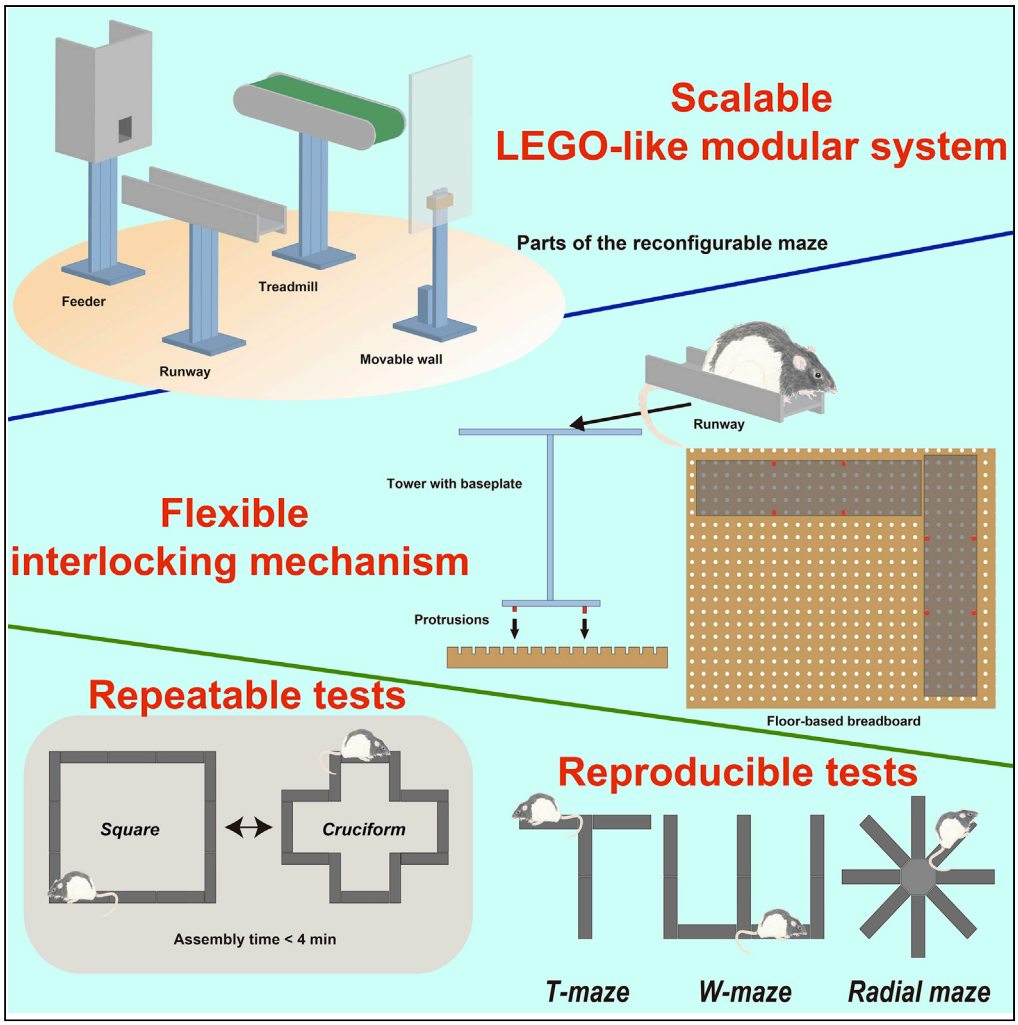

Satoshi Hoshino, Riku Takahashi, Kana Mieno, Yuta Tamatsu, Hirotsugu Azechi, Kaoru Ide, Susumu Takahashi

stakahas@mail.doshisha.ac.jp

HIGHLIGHTS

The reconfigurable maze enables flexibly in building a variety of maze paths

The maze ensures reproducibility, repeatability, and scalability

The maze does not impair spatial navigational behavior or neuronal activity

Various tests of learning and memory can be conducted in a single environment

Hoshino et al., iScience *23*, 100787
January 24, 2020
https://doi.org/10.1016/j.isci.2019.100787

iScience

CellPress

Article

The Reconfigurable Maze Provides Flexible, Scalable, Reproducible, and Repeatable Tests

Satoshi Hoshino,[1] Riku Takahashi,[1] Kana Mieno,[1] Yuta Tamatsu,[1] Hirotsugu Azechi,[1] Kaoru Ide,[1] and Susumu Takahashi[1,2,*]

SUMMARY

Multiple mazes are routinely used to test the performance of animals because each has disadvantages inherent to its shape. However, the maze shape cannot be flexibly and rapidly reproduced in a repeatable and scalable way in a single environment. Here, to overcome the lack of flexibility, scalability, reproducibility, and repeatability, we develop a reconfigurable maze system that consists of interlocking runways and an array of accompanying parts. It allows experimenters to rapidly and flexibly configure a variety of maze structures along the grid pattern in a repeatable and scalable manner. Spatial navigational behavior and hippocampal place coding were not impaired by the interlocking mechanism. As a proof-of-principle demonstration, we demonstrate that the maze morphing induces location remapping of the spatial receptive field. The reconfigurable maze thus provides flexibility, scalability, repeatability, and reproducibility, therefore facilitating consistent investigation into the neuronal substrates for learning and memory and allowing screening for behavioral phenotypes.

INTRODUCTION

Several shapes of mazes such as the T-maze (Small, 1901; Dudchenko, 2001), plus maze (Olton and Feustle, 1981), radial arm maze (Olton and Samuelson, 1976; Olton et al., 1978), and figure-8 maze (Wood et al., 2000) have been designed as behavioral tests to assess the performance of working (Dudchenko, 2004), reference (Olton and Paras, 1979; Xu et al., 2019) and episodic-like memory (Babb and Crystal, 2005), and spatial navigation (O'Keefe and Nadel, 1978), as well as for studying anxiety (Walf and Frye, 2007). As individual tests of learning and memory, all have pros and cons (Andersen et al., 2009). To compensate for the disadvantages, evidence from a battery of maze tests is usually accumulated to understand specific learning and memory (Tecott and Nestler, 2004). However, each test is often conducted in a different real or virtual experimental room because conventional mazes cannot be easily rebuilt in a systematically arranged manner. The details of the maze structure, including shape, coordination, and dimensions, are crucial aspects of the test results, whereas the structures themselves cannot be precisely reproduced in different laboratories in a repeatable way. Thus, conventional maze tests lack reproducibility and repeatability.

Place cells found in the hippocampus encode an animal's location and are deeply involved in spatial navigation ability (O'Keefe and Nadel, 1978). Place coding responds dramatically to changes in the surrounding environment (Muller and Kubie, 1987), suggesting that even if an animal experiences a single maze set inside different rooms, the hippocampus may generate different cognitive maps for each room, despite the mazes having identical shapes. On the other hand, conventional visual-based virtual reality (VR) systems can realize unlimited shapes of mazes in visual space. However, the lack of non-visual sensory feedback in passive VR results in altered neuronal responses. Furthermore, it forces animals to be partially or fully immobilized because one of the best applications of VR is to monitor neuronal activity from two-photon calcium imaging during the spatial navigation of head-fixed animals. For instance, a fraction of place cells reduced their firings in the spatial receptive field apparently because of the loss of vestibular feedback in the VR (Aronov and Tank, 2014). These altered neuronal responses impede detailed interpretations of the learning and memory mechanisms involved in maze tests.

Here we develop a maze system that overcomes most of these limitations by allowing the reconfiguration of the shape of the maze in a single physical environment. We demonstrate the use of the reconfigurable maze system to replicate existing mazes, including the T-maze, plus maze, W-maze, figure-8 maze, and radial arm maze. We also investigate the spatial navigational behavior and coding of the hippocampal

[1]Laboratory of Cognitive and Behavioral Neuroscience, Graduate School of Brain Science, Doshisha University, Kyotanabe City, Kyoto 610-0394, Japan

[2]Lead Contact

*Correspondence: stakahas@mail.doshisha.ac.jp

https://doi.org/10.1016/j.isci.2019.100787

place cells of rats to address concerns over possible distortions caused by the interlocking mechanisms and perform a novel experiment that morphs the shape of the maze. Together, these contribute to deciphering the neuronal underpinning of spatial navigation.

RESULTS

Implementation of the Reconfigurable Maze

We developed a maze system that enables the reconfiguration of the shape of the maze in a single physical environment using interlocking runways. Figure 1 demonstrates the existing standard mazes configured by our maze system in an enclosure, namely, the T-maze, W-maze, figure-8 maze, plus maze, and radial arm maze. The runways are each placed atop towers with baseplates (Table S1); these baseplates have protrusions that connect to a grid of holes in a floor-based breadboard (Figure 1F). The insertion of the protrusions into the breadboard connection enables coordination with the grid pattern and minimizes the swinging of the runways resulting from the movement of the animal (Figure 1G). Similarly, an array of accompanying parts, including feeders, movable walls, and treadmills placed atop towers of their own, can also be attached on the breadboards. Thus, the feeder can be placed by the side of any runway to change the reward location (Figure 1H, arrows). The movable wall can be placed at any of the interlocking gaps between runways as a dead end to dynamically control possible running paths (Figure 1H, arrowheads), and any runway can be replaced by the treadmill (Figure 1H, double arrowheads). Moreover, the shut-off sensor can be attached alongside any runway to signal a triggering event to the feeders and treadmills (Figure 1H, dashed arrows). Placing these interlocking parts onto the grid pattern enables the experimenters, even if they are not familiar with the maze, to precisely reproduce a variety of coordinated patterns of mazes for a brief period in a repeatable manner in a single physical environment. The maze also provides a scalable experimental setup because the complexity and the area of the maze is incrementally expandable by adding extra parts. When the morphing of a maze from square to cruciform was timed the time it took beginners to assemble a maze was not significantly different from the assembly time of experts who had used the reconfigurable maze daily over 3 months (3 experts: 131 $\pm$ 9 s; 3 beginners: 158 $\pm$ 12 s [mean $\pm$ SEM]; Figure 1J, Video S1, S2, S3, S4, S5, and S6). Runway sections with tall sidewalls (35 cm height) for reducing fear can be placed to test anxiety (Figure S1). Instead of runways, open platforms can also be embedded into the maze, which enables the plus maze and radial arm maze to be configured (Figures 1D and 1E). Furthermore, the scheduler for the timing of sensors and actuators installed in the accompanying parts allows the experimenter to design several behavioral tasks, even within a single maze shape. Such flexible maze design also allows experimenters to rapidly select the tasks best matched to the needs of a particular experiment during preliminary studies. In accordance with this flexible design principle, we also developed a small version of the reconfigurable maze system for mice (Figure 1I, Table S2). Using the mouse version, we could also configure existing standard mazes, namely, the T-maze, W-maze, figure-8 maze, and plus maze (Figure S2). The assembly time for morphing a maze shape from square to T between experts and beginners was not significantly different (3 experts: 204 $\pm$ 15 s; 3 beginners: 186 $\pm$ 11 s [mean $\pm$ SEM]; Figure 1K), further demonstrating the usability of our system for screening behavioral phenotypes in mice.

Interlocking Gaps Do Not Alter Navigational Behavior

To manufacture the interlocking parts at a reasonable cost or by hand, a short gap between runways ($\sim$1 cm) (Figure 2A) is a prerequisite margin for the parts to interlock. Ideally, perfectly manufactured parts with a precision under 1 mm would not require these gaps as margins; however, such high-precision manufacturing is expensive and does not permit the use of low-precision handcrafted parts. When the gaps are not included as a margin, runways manufactured with lower precision (>1 cm) will overlap if the location of the runway is only slightly shifted, as shown in Figure S3.

We next answered the question of whether this gap affects animal behavior. Four rats were trained to smoothly run along a square-shaped maze in a clockwise direction. The running speed at the gaps did not abruptly change from the running speed between gaps (Figure 2B). Incidences of abrupt changes in the head direction were significantly lower at the gaps than between gaps (Figure 2C). These results suggest that the gaps did not distort normal rats' behaviors. To corroborate the result, we prepared two gapless runways the total lengths (149 cm long) of which were the same as those of the three interlocking runways, including the gaps between the sections. We then replaced three runway sections at the top or bottom of the square-shaped maze with a single runway without gaps (Figure S4A). Five rats were trained to run on the mazes, with or without gaps, over a 20-min interval. Both running speed and head direction on

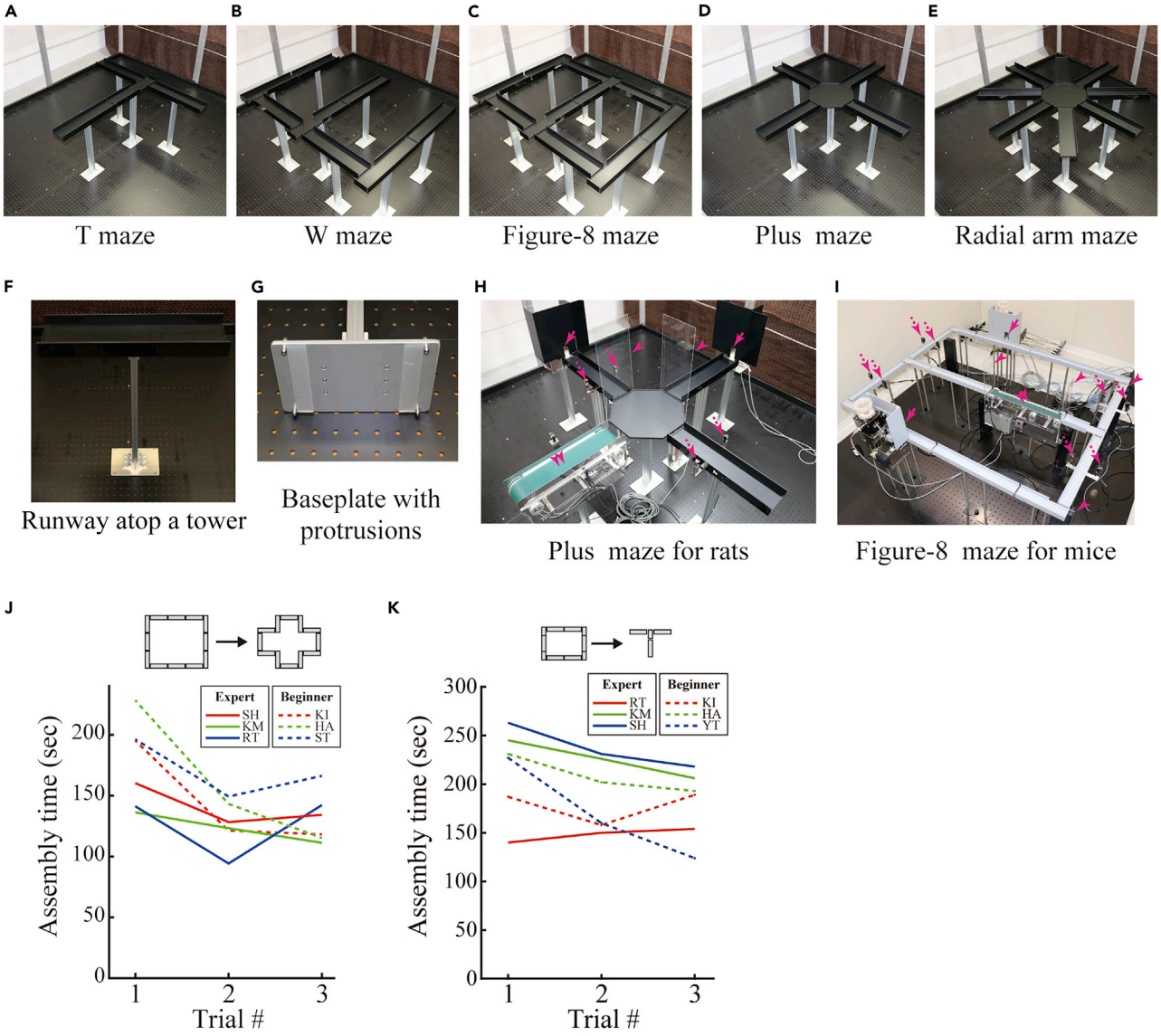

Figure 1. The Reconfigurable Maze

Figure360▷ For a Figure360 author presentation of this figure, see https://doi.org/10.1016/j.isci.2019.100787.

(A–E) The maze can be configured to form T (A), W (B), figure-8 (C), plus (D), and radial arm (E) mazes in a single enclosure.

(F) Runway sections are placed atop towers.

(G) The baseplate of each tower has four protrusions that coordinate the placement of the section on the breadboard in a flexible, repeatable way.

(H) Configured plus maze for rats with two feeders (arrows), two movable walls (arrowheads), one treadmill (double arrowhead), and two shut-off sensors (dashed arrows).

(I) Small version of the reconfigurable maze for mice, configured as a figure-8 maze with two feeders (arrows), two movable walls (arrowheads), one treadmill (double arrowhead), and two shut-off sensors (dashed arrows).

(J) Assembly time of the rat version of the reconfigurable maze for morphing the shape from square to cruciform. Performance improved with consecutive trials in a day (performance versus trial: $F_{2,8} = 7.453$, $p = 0.0149$), but not with expertise (expert/beginner) (performance versus expertise: $F_{1,4} = 5.654$, $p = 0.0762$). There was no significant interaction between expertise and experience in a day (expertise versus trial: $F_{2,8} = 0.320$, $p = 0.735$). Two-way mixed ANOVA was used.

(K) Assembly time of the mouse version of the reconfigurable maze for morphing the shape from a rectangle to a T. There was no significant difference between performance and consecutive trials in a day (performance versus trial: $F_{2,8} = 3.997$, $p = 0.0625$) or expertise (expert/beginner) (performance versus expertise: $F_{1,4} = 0.351$, $p = 0.58$). There was no significant interaction between expertise and experience in a day (expertise versus trial: $F_{2,8} = 0.658$, $p = 0.543$).

Two-way mixed ANOVA was used.

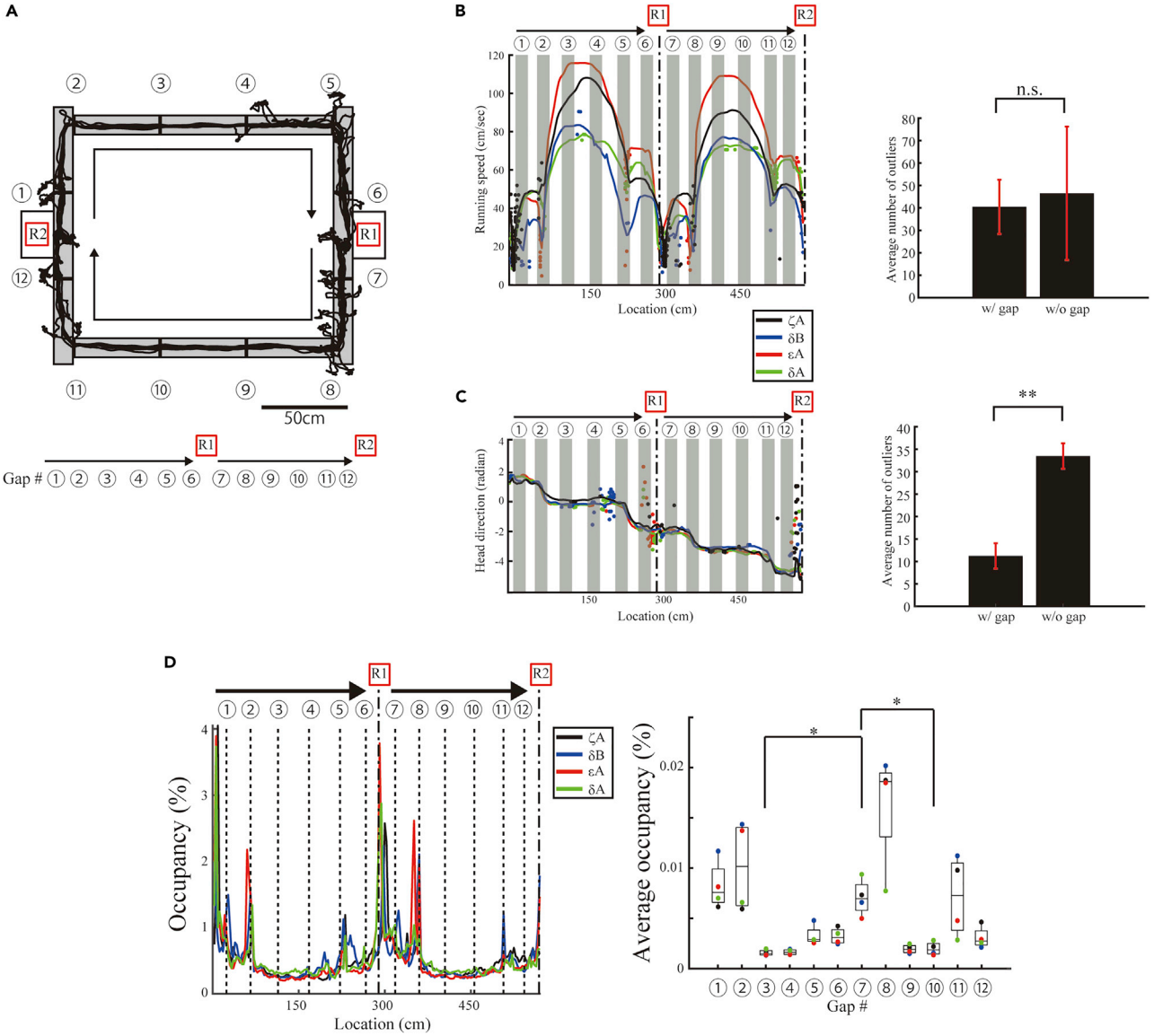

Figure 2. Interlocking Gaps Do Not Alter Navigational Behavior

(A) Schematics of the square-shaped maze test. An example running trajectory of a rat is superimposed on the maze. The numbers indicate gap locations. R1 and R2 indicate food dispensers. Linearized gap locations are illustrated at the bottom.

(B and C) Left, the average running speed and head direction of four rats as a function of the linearized location. The dots indicate the location of outliers for each lap. Right, the average number of outliers on the regions around the gap (gray shaded areas) and others (running speed: $t = -0.19$, $df = 6$, $p = 0.86$; head direction: $t = -5.53$, $df = 6$, $p = 0.0015$, two-tailed paired t test). $^{**}p < 0.01$, n.s.: $p > 0.05$. Error bars indicate SEM.

(D) Left, the percentage of the occupancy time over the entire maze as a function of the linearized location of four rats. Right, the median percentage of the occupancy time at gap locations (median, first and third quartiles, minimum, and maximum indicated). The rats preferentially slow down at gap #7 as compared with gaps #3 and #10, which are located at the top and bottom of the maze ($F_{1,3} = 152.69$, $p = 0.0011$; gap #7 versus #3: $p = 0.049$; gap #7 versus #10: $p = 0.030$, One-way repeated-measures ANOVA with post hoc Tukey's honestly significant difference test). $^{*}p < 0.05$

the gaps were not significantly different from those on the corresponding portions of the single runway without gaps (Figures S4B and S4C).

As shown from the trajectory (Figure 2A) and abrupt changes in the head direction (Figure 2C), the rats appeared to frequently exhibit exploratory behaviors at preferred locations (Hu and Amsel, 1995). To examine whether such exploration is preferentially observed at gap locations, four rats were trained to run in a clockwise direction on a square-shaped maze configuration. All rats sometimes paused and exhibited

exploratory behaviors around food dispensers or corners. Indeed, the occupancy time when the rats visited the gap location around a food dispenser (gap #7) was significantly longer than the occupancy time on two other gaps (gaps #3 and #10) (Figure 2D), suggesting that unidentified factors, excluding the gap presence, might also affect rats' behaviors around food dispensers or corners. In addition, it is well known that such exploratory behaviors modulate hippocampal neuronal activity (Gauthier and Tank, 2018). Thus, to exclusively examine the gap effects, we focused on the gaps (#3, #4, #9, and #10) between the three interlocking runways arranged in a straight line on the top and bottom sides of the square-shaped maze in the subsequent analyses.

Interlocking Gaps Do Not Alter Hippocampal Place Coding

To determine whether the gaps distort neuronal activity in terms of spatial navigation, we monitored the activity of 236 neurons from the hippocampal CA1 of both hemispheres of four rats running on the square-shaped maze in a clockwise direction (Figure 3A, Table S3). The average width of place fields of 62 place cells on the gaps settled between the 5^{th} and 95^{th} percentiles of distribution for shuffled data from the entire set of place fields (Figure 3B). Moreover, the number of place fields from the 62 place cells and the firing rate of multiunit activity in the hippocampal CA1 on the gaps did not change when compared with recordings taken between the gaps (Figures 3C and 3D). At the ensemble level, the trajectory decoded from the activity of simultaneously monitored place cells using a memoryless Bayesian decoder (Zhang et al., 1998) depicted a seamless path even on the gap locations (Figures 3E and 3F). Thus, both behavioral and neuronal responses at the gaps support the view that rats behave as if they perceive the interlocking gap and gapless portions on the runways similarly.

Rats and Mice Can Learn Spatial Alternation Tasks in the Reconfigured Maze

After the five rats became familiar with the square-shaped maze, the maze shape was morphed from square to figure-8 using the reconfigurable maze system. The rats were trained to alternate between left and right at the branchpoint of the central stem for 1 h per day over 5 days (Figure 4A). All rats gradually learned the spatial alternation task (Figure 4C). They achieved a mean score of greater than 80% correct choices over 50 consecutive trials on the second day. To demonstrate the usability of the attachable walls and treadmills, three rats were then tested on a delayed version of the spatial alternation task by partially reconfiguring the maze: a runway in the center of the stem in the figure-8-shaped maze was replaced by a treadmill (Figure 4B). To force the rats to run on the treadmill for a 7-s delay period, movable walls were set at the gaps in front and behind the treadmill. The rats achieved a mean score of greater than 70% correct choices over 50 consecutive trials at the beginning, and their performance improved after 10 days of testing (Figure 4D).

After three mice were familiar with the linear track and rectangular maze in the mouse version of the reconfigurable maze, the maze shape was morphed to a T-maze (Figures 4E and 4F). The mice were trained to alternate between left and right at two branch points for 1 h per day over 5 days. All mice gradually learned the spatial alternation task (Figure 4G). They achieved a mean score of greater than 75% correct choices over 20 consecutive trials on the second day. These results and maze reconfigurations demonstrate that the reconfigurable maze system can consistently replicate the existing standard mazes and serve as tests of spatial learning and memory.

Place Field Remapping during the Maze Morphing Experiment

Several lines of evidence suggest the hippocampal place coding partially or completely changes in response to external or internal cues (Muller and Kubie, 1987; Leutgeb et al., 2005). This phenomenon is called the remapping of place fields. To demonstrate the repeatability and reproducibility of our reconfigurable maze system over existing mazes, we provide here a novel morphing experiment to examine the remapping of place fields between different shapes of a maze with an identical path length when the maze shape morphs from square to cruciform to square. As the cruciform maze is an internal structure of the square maze, the total path length does not change during morphing. Moreover, the four outermost runways of the cruciform maze physically overlap with the path of the square-shaped maze. As our maze realizes the morphing in one enclosure, it enables the identification of factors influencing hippocampal place coding: path integration and spatial reference frame (Figure 5A).

To examine the remapping of the place fields, we examined 129 place cells monitored from the dorsal hippocampal CA1 of four rats. The total path length of the runway and available external landmarks in the

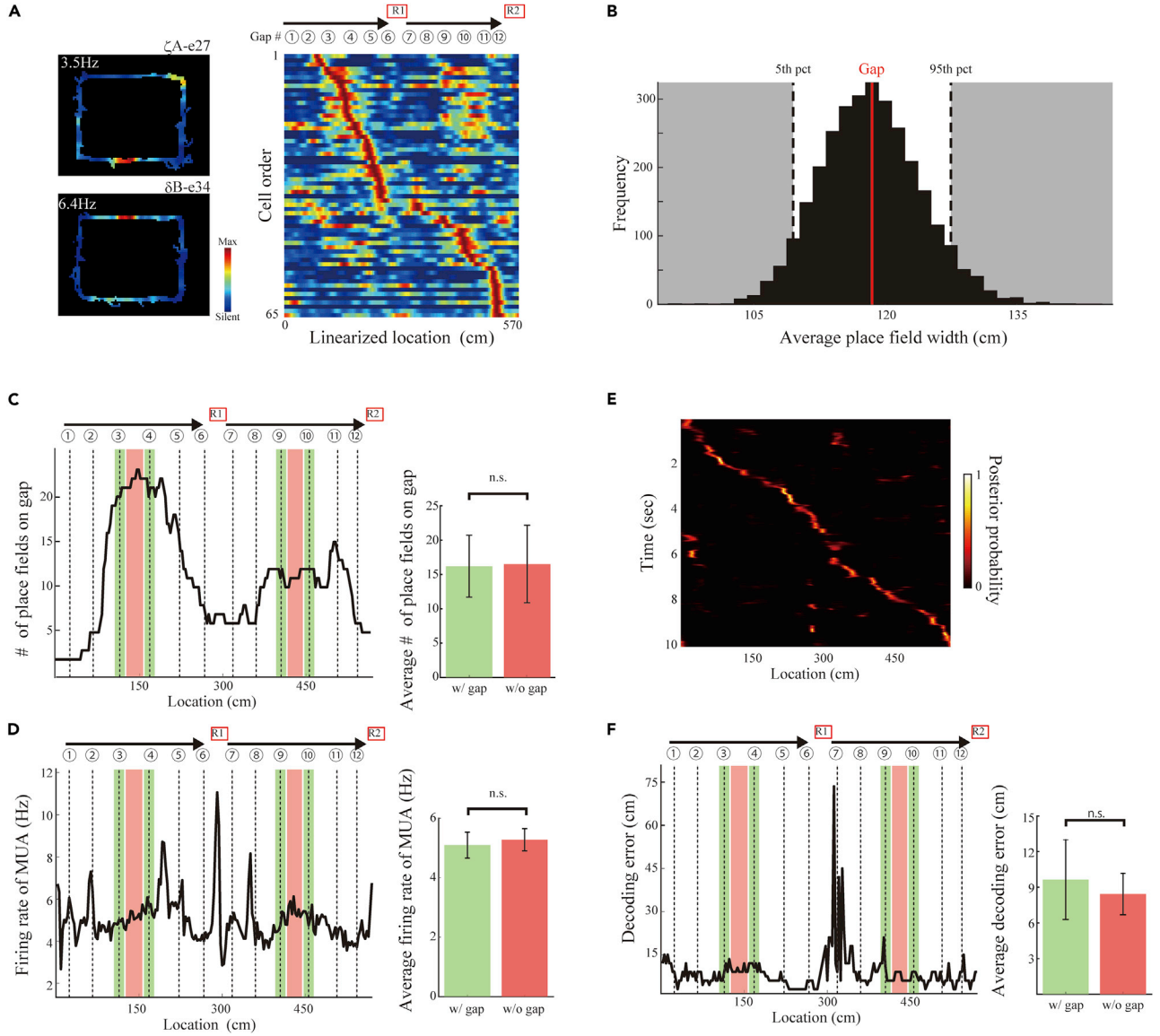

Figure 3. Interlocking Gaps Do Not Alter Hippocampal Place Coding

(A) Left, normalized firing rate map of two representative place cells that have place fields around gap locations in the hippocampal CA1 on the square-shaped maze configuration. Right, normalized firing rate maps of 65 hippocampal place cells simultaneously monitored from a rat (ζA) ordered by the latency of their peak firing rates. Each line is a single unit. Gap locations are indicated at the top. Red indicates maximum firing rates, and blue indicates silent.

(B) Distribution of the average width of place fields randomly shuffled from the original sample covering the gaps (3,000 shuffles). Red line indicates the average width of the place fields on the gaps. Dotted lines indicate 5th and 95th percentiles for the shuffled data.

(C and D) Left, the number of place fields (C) and the firing rate of multi-unit activity (MUA) in the hippocampal CA1 (D) as a function of linearized location on the square-shaped maze. Right, the average number of place fields (C) ($z = 0.14$, $p = 0.89$) and the average firing rate of MUA ($z = -1.51$, $p = 0.13$) on the gaps (#3, 4, 9, 10) (green shaded area) and between them (orange shaded area).

(E) Representative posterior probability of locations decoded by the Bayesian decoder from 89 simultaneously monitored cells. Values are indicated by the color bar (right).

(F) Left, the difference between actual and decoded locations as a function of linearized location on the square-shaped maze. Right, the average difference between actual and decoded locations on the gaps (#3, 4, 9, 10) (green shaded area) and between them (orange shaded area) ($z = 1.34$, $p = 0.18$). Bin width is set at 3 cm.

All error bars indicate SEM. All were from two-tailed Wilcoxon rank-sum test, n.s.: $p > 0.05$.

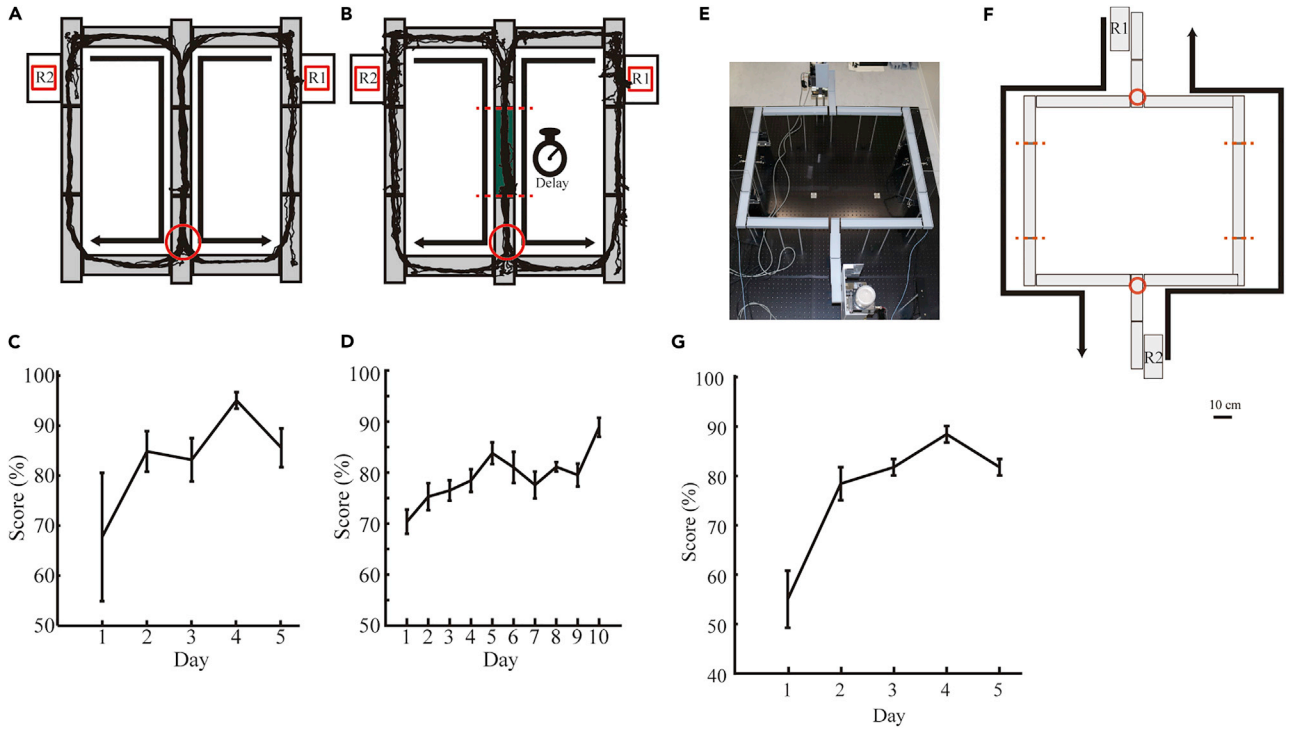

Figure 4. Rats and Mice Can Learn to Navigate the Configured Mazes

(A) Schematic of the figure-8-shaped maze created using the rat version of the reconfigurable maze. Example animal trajectories are superimposed on top of the maze. The red circle indicates a branchpoint where the rat must decide which direction to turn.

(B) Same as in (A) but with a treadmill (green). Red dashed lines indicate the gap locations where movable walls are placed to force the rats to run on the treadmill for a delay period.

(C) Spatial alternation task performance improved with experience (performance versus testing day: $F_{1,\ 4} = 795.9$, $p < 10^{-5}$).

(D) Performance of the delayed version of the spatial alternation task of rats improved with experience (performance versus testing day: $F_{1,2} = 531.8$, $p = 0.0019$). All were from one-way repeated-measures ANOVA. Error bars indicate SEM.

(E) Top view of the configured double T-maze using the mouse version of the reconfigurable maze.

(F) Schematics of the double T-maze. Example mouse trajectories are superimposed on the maze. Arrow marks the running directions from the food dispensers (R1/R2). The red circles indicate branch points where the mice must decide which direction to turn. Red dotted lines indicate the locations where the movable walls are placed to prevent a reverse run.

(G) Spatial alternation task performance of mice improved with experience (performance versus testing day: $F_{1,2} = 7320$, $p = 0.000136$). One-way repeated-measures ANOVA was used. Error bars indicate SEM.

mazes were nearly identical across maze shape morphs, whereas the spatial correlation of the firing rate map of place cells within the overlapping runways in the square-shaped maze between the first and second exposures was significantly larger than that between the square-shaped maze and the cruciform maze (Figures 5B and 5C). This suggests that the maze shape can be a cue capable of inducing remapping of the location of place fields as a spatial reference frame. Moreover, the difference in the maximum firing rate of place fields within the overlapping runways in the square-shaped maze between the first and second exposures was similar to that between the square-shaped maze and the cruciform maze (Figures 5B and 5D). These results suggest that maze morphing from square to cruciform is represented by a difference in place field locations without a change in place field firing rate.

DISCUSSION

We demonstrate our reconfigurable maze system's ability to provide flexible, scalable, repeatable, and reproducible tests by configuring standard existing mazes in a single real environment and by examining spatial navigational behavior and neuronal activity during learning and memory performances in the mazes. Our maze system has the potential to become an invaluable, scalable tool for the study of learning and memory, including working and reference memory, spatial navigation, and decision-making, as well as anxiety. Using the reconfigurable maze, experimenters can consistently replicate a variety of mazes in their

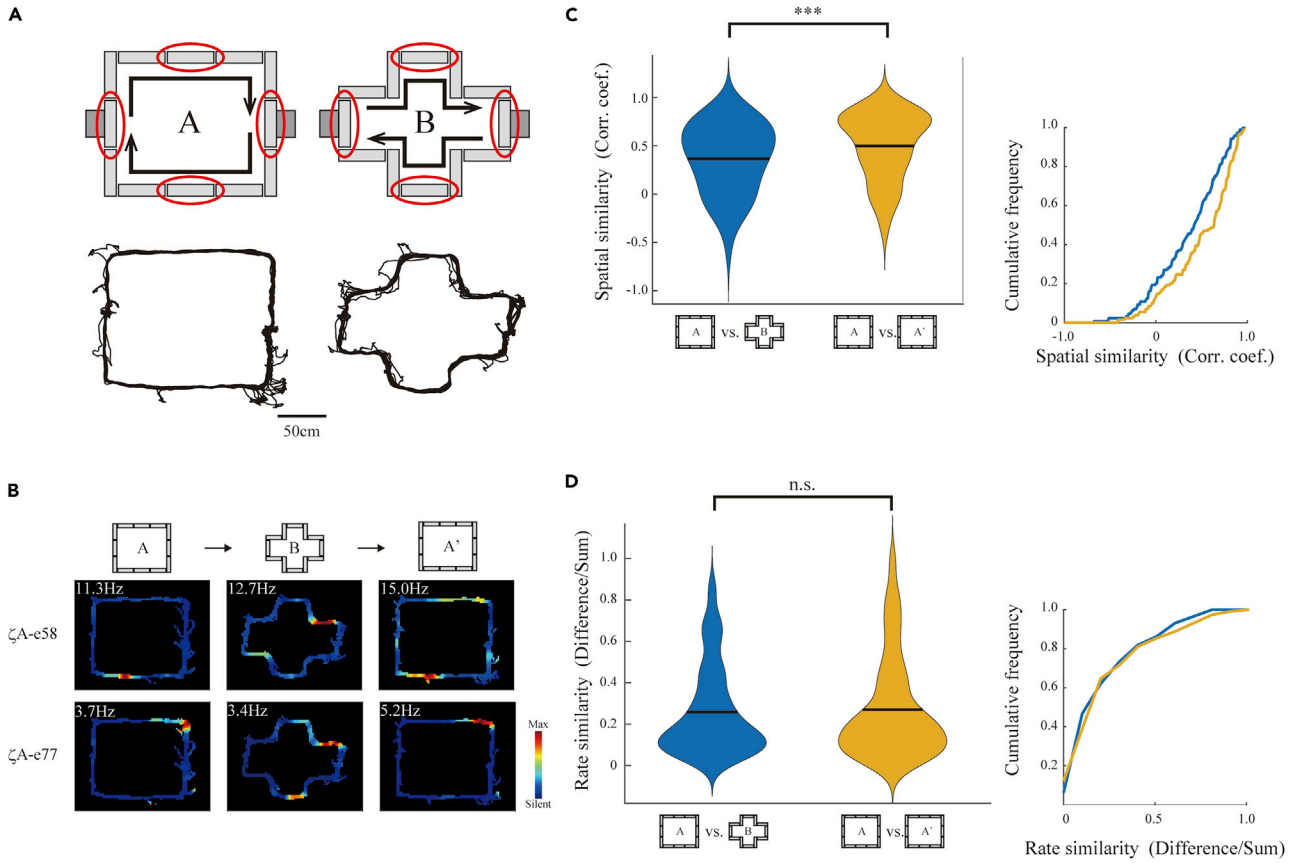

Figure 5. Place Field Remapping during the Maze Morphing Experiment

(A) Schematics of square and cruciform mazes configured by our system (top) and the representative running trajectory of a rat (bottom). The runways enclosed by red circles were not moved during the morphing experiment.

(B) Representative change of the place field of a place cell recorded from a rat (ζA) during maze morphing. The maximum firing rate is displayed at the top left corner.

(C and D) Violin plots of spatial similarity as the spatial correlation of the firing rate map (C) ($z = -3.98$, $p = 10^{-4}$) and rate similarity as firing rate difference within place fields (D) ($z = -0.60$, $p = 0.55$) between the square maze and cruciform maze, and between the first and second exposures of the square maze (left). The bar indicates the median. Surrounding each side is a rotated kernel density plot. Their cumulative frequency is graphed to the right.

All were from two-tailed Wilcoxon signed-rank test. ***$p < 0.001$, n.s.: $p > 0.05$.

laboratory, and the position of the maze parts can be reconfigured for a brief period in a repeatable manner to test several task performances in a single physical environment.

Currently, a variety of maze tests are routinely used to gain a greater understanding of learning and memory in animals and for screening behavioral phenotypes in animal models of diseases. Although evidence is being accumulated, it is not necessarily available to contribute to our understanding of learning and memory mechanisms in the brain, because the underlying neuronal signatures are not necessarily similar, even when identical maze shapes are used across different conditions. For instance, if a behavioral phenotype for spatial memory deficits emerged in two maze tests, each conducted in a different room, the tests may only specifically show the remapping of hippocampal place coding across the different rooms, as demonstrated in the maze morphing experiment of the present study. Indeed, recent studies suggest that place cell activity sequences are linked to future planning (Pfeiffer and Foster, 2013) and episodic-like memory retrieval (Takahashi, 2015), as well as neurodegenerative diseases (Cheng and Ji, 2013). Therefore, such neuronal dissociations should be minimized in a comparative study across maze tests. Place cells show an irregular firing pattern in passive VR experiments (Aronov and Tank, 2014). Therefore, we designed our maze based on the concept that various shapes can be constructed in a single real environment, where several types of learning and memory tests can be performed. Recently developed active VR can markedly minimize such dissociations, specifically for proximal cues (Aronov and Tank, 2014; Stowers et al., 2017).

Although our maze system and the active VR are not exclusive, the combination will enable the production of unlimited experimental situations without the neuronal distortions arising from both proximal and distal cues in the near future.

Our reconfigurable maze system is compatible with techniques for monitoring neuronal activity such as extracellular multiple single-unit recording (Wilson and McNaughton, 1993) and single-photon calcium imaging (Ziv et al., 2013) for freely behaving rats or mice. As demonstrated by the remapping of place fields across morphed mazes, the combination must be accelerated to allow understanding of the neuronal underpinning of learning and memory. Furthermore, our maze enables rapid prototyping of tasks by reconfiguring the coordination of the parts, including runways, rewards, and obstacles, within a few minutes, accelerating studies on learning and memory.

The reconfigurable maze is thus a promising maze platform for testing the performance of learning and memory, including working, reference and episodic memory, decision-making, spatial navigation, and anxiety, as well as for screening behavioral phenotypes of mice, including transgenic models of disease.

Limitations of the Study

The initial setup cost and laboratory space for introducing the reconfigurable maze may be barriers to widespread distribution. However, the scalable features minimize these barriers. For instance, a minimal setup realized by removing optional modules from the full configuration (demonstrated by a square-shaped maze without movable walls or shut-off sensors) will reduce the cost. In addition, the modular architecture allows the configuration of small mazes to fit limited laboratory space. Although the minimal setup may not be a compelling reason for laboratories to invest in the reconfigurable maze, the complexity can be expanded incrementally by adding supplementary parts. Moreover, the setup and validation for novel configured mazes within a laboratory may be time consuming. Provided that the reconfigurable maze will be widely distributed and standardized, the overall cost will be lowered and information resources describing how to set up new configurations of the maze and validate their performance for specific aims will be shared between researchers. In this way, implementation of the reconfigurable maze will ensure reproducibility and repeatability.

Despite its flexibility, reproducibility, repeatability, and scalability, our maze has a few limitations. Although oblique runways at an angle of 45° could be embedded into our maze as demonstrated by the configured radial arm maze (Figure 1E), the angle cannot be flexibly modified because the coordinated grid assignment of the parts requires the runways to be placed at a fixed angle. Unlike the recently developed honeycomb maze (Wood et al., 2018), the tower supporting the runway cannot be raised and lowered automatically. Although adjustable mechanisms are capable of overcoming those limitations, they increase the damage rate of the physical system during behavioral and neuronal recordings, reducing the major advantage of reproducibility and repeatability.

METHODS

All methods can be found in the accompanying Transparent Methods supplemental file.

DATA AND CODE AVAILABILITY

The detail of the maze parts is freely available (https://github.com/TakahashiLab/ReconfigurableMazeParts). The controlling software is also freely available (https://github.com/TakahashiLab/ReconfigurableMazeGUI).

SUPPLEMENTAL INFORMATION

Supplemental Information can be found online at https://doi.org/10.1016/j.isci.2019.100787.

ACKNOWLEDGMENTS

This work is supported by the JSPS KAKENHI (16H06543, 16H02840, and 19H01131) to S.T.

AUTHOR CONTRIBUTIONS

S.T. conceived the project. S.H. developed control software. S.H., K.M., R.T., and Y.T. performed behavioral experiments. H.A. and K.I. performed the histological verification. S.H., H.A., and K.I. made apparatus. S.H.

performed electrophysiological experiments. S.H. and S.T. performed surgery, data analyses, and wrote the manuscript.

DECLARATION OF INTERESTS

S.T. is an inventor on Japanese unexamined patent application publication (No. P2019-115315A, applicant: Doshisha University) pertaining to the reconfigurable maze. All remaining authors declare no conflict of interest.

Received: October 16, 2019
Revised: November 25, 2019
Accepted: December 13, 2019
Published: January 24, 2020

REFERENCES

Andersen, P., Morris, R., Amaral, D., Bliss, T., and O'Keefe, J. (2009). The Hippocampus Book (Oxford University Press).

Aronov, D., and Tank, D.W. (2014). Engagement of neural circuits underlying 2d spatial navigation in a rodent virtual reality system. Neuron *84*, 442–456.

Babb, S.J., and Crystal, J.D. (2005). Discrimination of what, when, and where: implications for episodic-like memory in rats. Learn. Motiv. https://doi.org/10.1016/j.lmot.2005.02.009.

Cheng, J., and Ji, D. (2013). Rigid firing sequences undermine spatial memory codes in a neurodegenerative mouse model. Elife *2013*, 1–26.

Dudchenko, P.A. (2001). How do animals actually solve the T maze? Behav. Neurosci. *115*, 850–860.

Dudchenko, P.A. (2004). An overview of the tasks used to test working memory in rodents. Neurosci. Biobehav. Rev. *28*, 699–709.

Gauthier, J.L., and Tank, D.W. (2018). A dedicated population for reward coding in the hippocampus. Neuron *99*, 179–193.e7.

Hu, D., and Amsel, A. (1995). A simple test of the vicarious trial-and-error hypothesis of hippocampal function. Proc. Natl. Acad. Sci. U S A *92*, 5506–5509.

Leutgeb, S., Leutgeb, J.K., Barnes, C.A., Moser, E.I., McNaughton, B.L., and Moser, M.B. (2005). Independent codes for spatial and episodic memory in hippocampal neuronal ensembles. Science *309*, 619–623.

Muller, R.U., and Kubie, J.L. (1987). The effects of changes in the environment on the spatial firing of hippocampal complex-spike cells. J. Neurosci. *7*, 1951–1968.

O'Keefe, J., and Nadel, L. (1978). The Hippocampus as a Cognitive Map (Oxford University Press).

Olton, D.S., and Feustle, W.A. (1981). Hippocampal function required for nonspatial working memory. Exp. Brain Res. *41*, 380–389.

Olton, D.S., and Paras, B.C. (1979). Spatial memory and hippocampal function. Neuropsychologia *17*, 669–682.

Olton, D.S., and Samuelson, R.J. (1976). Remembrance of places passed: spatial memory in rats. J. Exp. Psychol. Anim. Behav. Process. https://doi.org/10.1037/0097-7403.2.2.97.

Olton, D.S., Walker, J.A., and Gage, F.H. (1978). Hippocampal connections and spatial discrimination. Brain Res. *139*, 295–308.

Pfeiffer, B.E., and Foster, D.J. (2013). Hippocampal place-cell sequences depict future paths to remembered goals. Nature *497*, 74–79.

Small, W.S. (1901). Experimental study of the mental processes of the rat. II. Am. J. Psychol. https://doi.org/10.2307/1412534.

Stowers, J.R., Hofbauer, M., Bastien, R., Griessner, J., Higgins, P., Farooqui, S., Fischer, R.M., Nowikovsky, K., Haubensak, W., Couzin, I.D., et al. (2017). Virtual reality for freely moving animals. Nat. Methods *14*, 995–1002.

Takahashi, S. (2015). Episodic-like memory trace in awake replay of hippocampal place cell activity sequences. Elife *4*, e08105.

Tecott, L.H., and Nestler, E.J. (2004). Neurobehavioral assessment in the information age. Nat. Neurosci. *7*, 462–466.

Walf, A.A., and Frye, C.A. (2007). The use of the elevated plus maze as an assay of anxiety-related behavior in rodents. Nat. Protoc. *2*, 322–328.

Wilson, M.A., and McNaughton, B.L. (1993). Dynamics of the hippocampal ensemble code for space. Science *261*, 1055–1058.

Wood, E.R., Dudchenko, P.A., Robitsek, R.J., and Eichenbaum, H. (2000). Hippocampal neurons encode information about different types of memory episodes occurring in the same location. Neuron *27*, 623–633.

Wood, R.A., Bauza, M., Krupic, J., Burton, S., Delekate, A., Chan, D., and O'Keefe, J. (2018). The honeycomb maze provides a novel test to study hippocampal-dependent spatial navigation. Nature *554*, 102–105.

Xu, H., Baracskay, P., O'Neill, J., and Csicsvari, J. (2019). Assembly responses of hippocampal CA1 place cells predict learned behavior in goal-directed spatial tasks on the radial eight-arm maze. Neuron *101*, 119–132.e4.

Zhang, K., Ginzburg, I., McNaughton, B.L., and Sejnowski, T.J. (1998). Interpreting neuronal population activity by reconstruction: unified framework with application to hippocampal place cells. J. Neurophysiol. *79*, 1017–1044.

Ziv, Y., Burns, L.D., Cocker, E.D., Hamel, E.O., Ghosh, K.K., Kitch, L.J., El Gamal, A., and Schnitzer, M.J. (2013). Long-term dynamics of CA1 hippocampal place codes. Nat. Neurosci. *16*, 264–266.

iScience, Volume *23*

Supplemental Information

The Reconfigurable Maze Provides Flexible, Scalable, Reproducible, and Repeatable Tests

Satoshi Hoshino, Riku Takahashi, Kana Mieno, Yuta Tamatsu, Hirotsugu Azechi, Kaoru Ide, and Susumu Takahashi

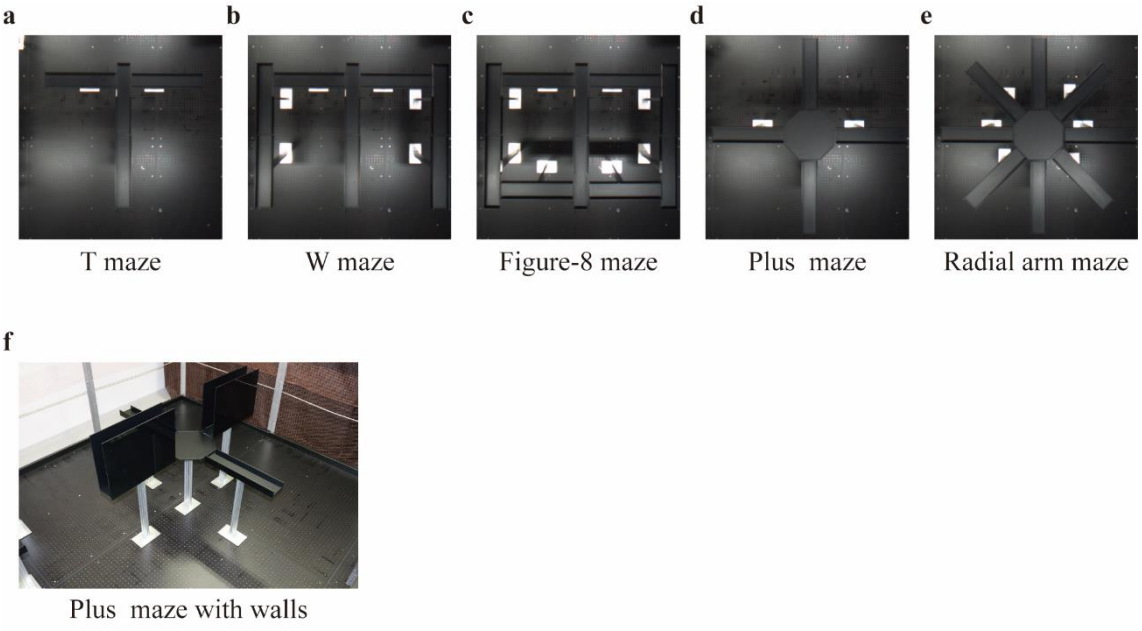

Figure S1. Top view of configured mazes, Related to Figure 1. (**a**–**e**) Top view of maze shape configured to T (**a**), W (**b**), figure-8 (**c**), plus (**d**), and radial arm (**e**) mazes in an enclosure. This view demonstrates that several shapes of the maze can be configured in the same space. (**f**) The plus maze configured with tall sidewalls for testing anxiety.

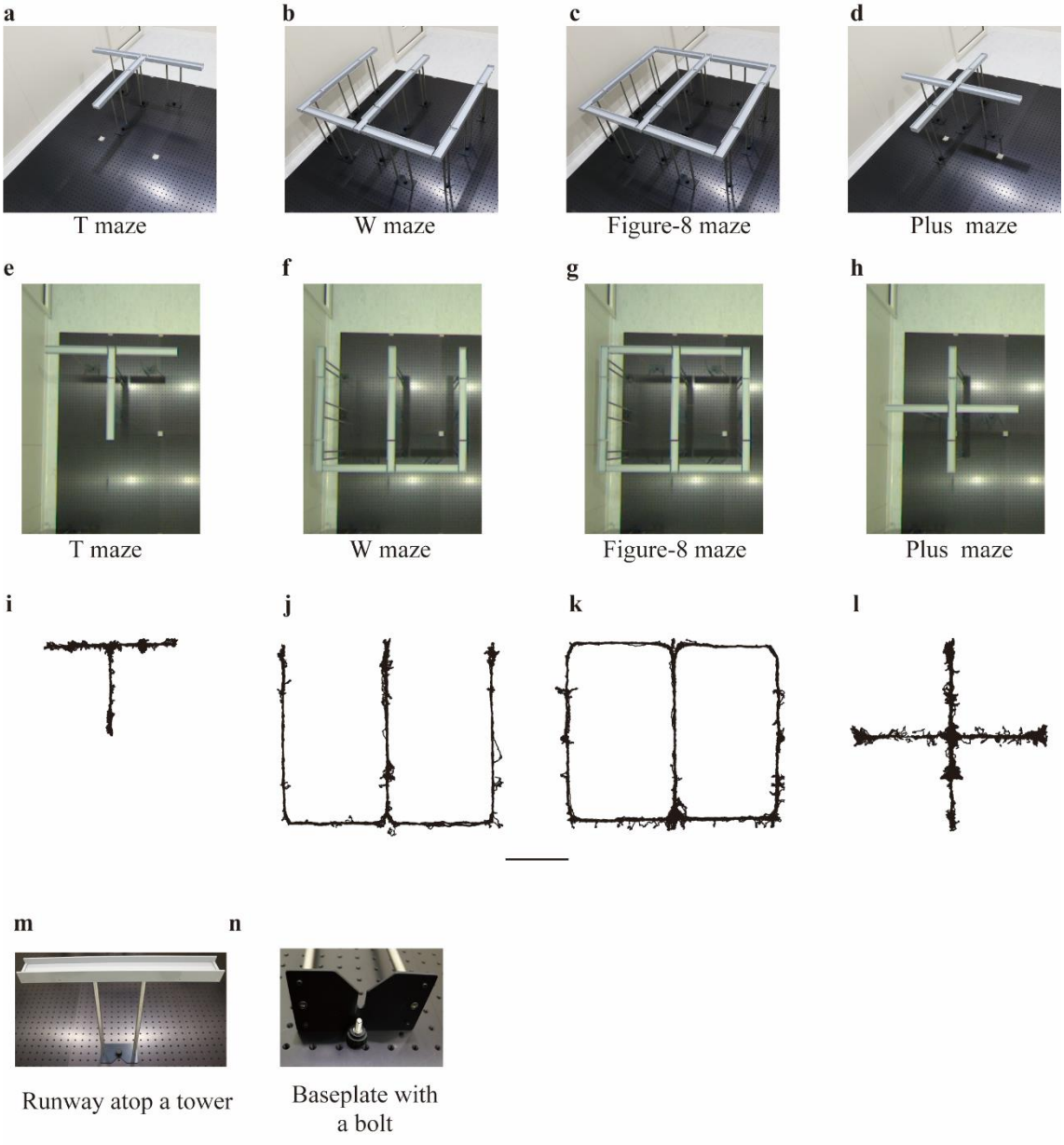

Figure S2. The reconfigurable maze for mice, Related to Figure 1. (**a**–**d**) The shape was configured to match T (**a**), W (**b**), figure-8 (**c**), and plus (**d**) mazes in an enclosure. (**e–h**) Top view of the mazes. Note that the central stem remains in the same position. (**i–l**) Example running trajectory of a mouse in each maze. Scale bar, 40 cm. (**m**) The runway is placed atop a tower on a breadboard with a grid of holes. (**n**) The baseplate of the tower is fixed by a bolt because the weight of the baseplate alone is too light to support the runway. The grid of the breadboard allows the flexible coordination of the runways and accessory parts in repeatable ways.

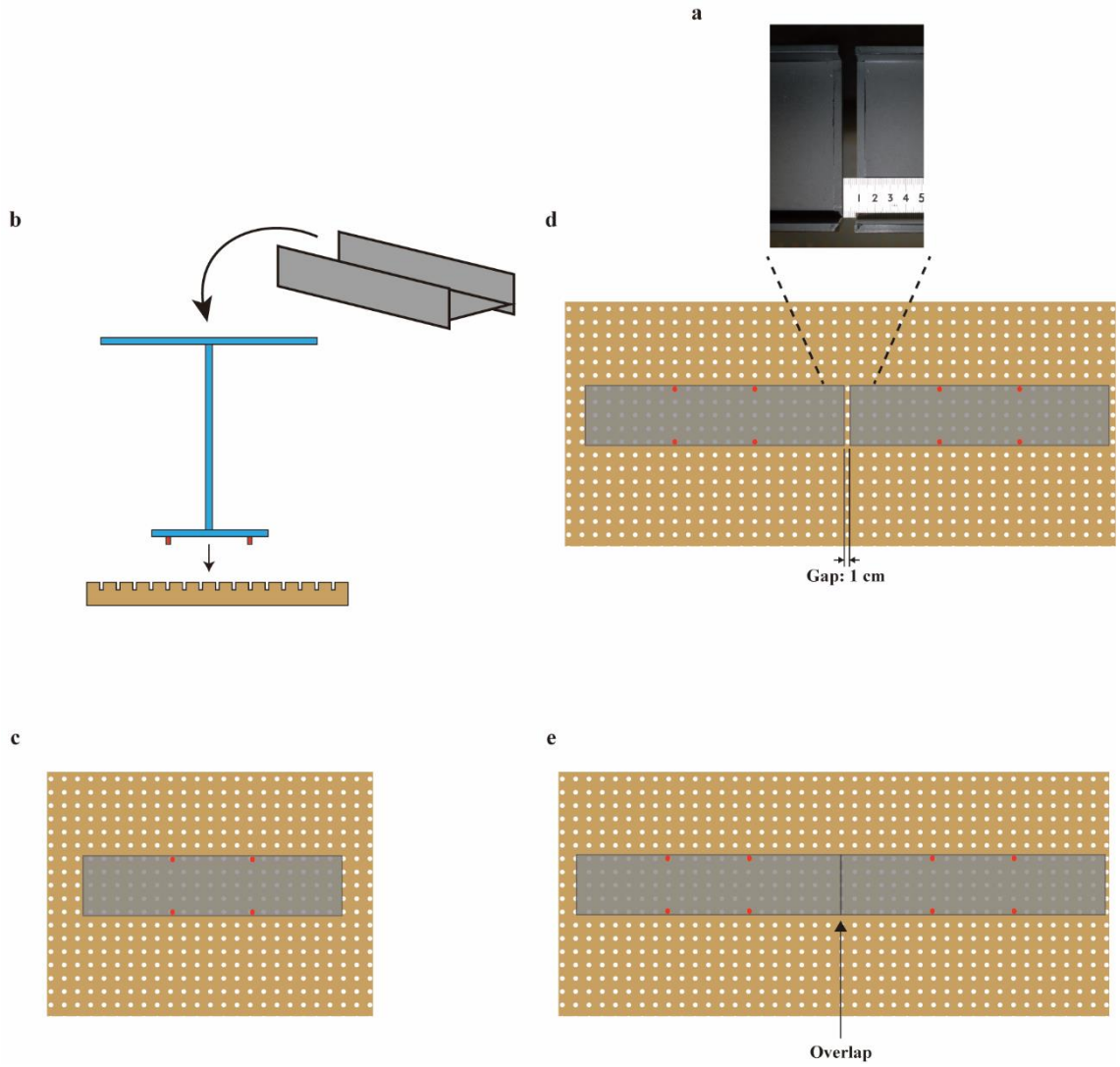

Figure S3. A short gap between runways is a prerequisite margin for the interlocking parts, Related to Figure 1. (**a**) Close-up photo showing the gap. (**b**) The runway (gray) is placed atop a tower (blue) on a breadboard (brown) with a grid of holes. The baseplate of the tower has protrusions (red) that coordinate the placement of the section on the breadboard. (**c**) Top view of a runway on the breadboard. (**d**) Two runways with a 1 cm gap. (**e**) This view demonstrates that the runways overlap only if the total dimensional error exceeds a precision of 1 cm.

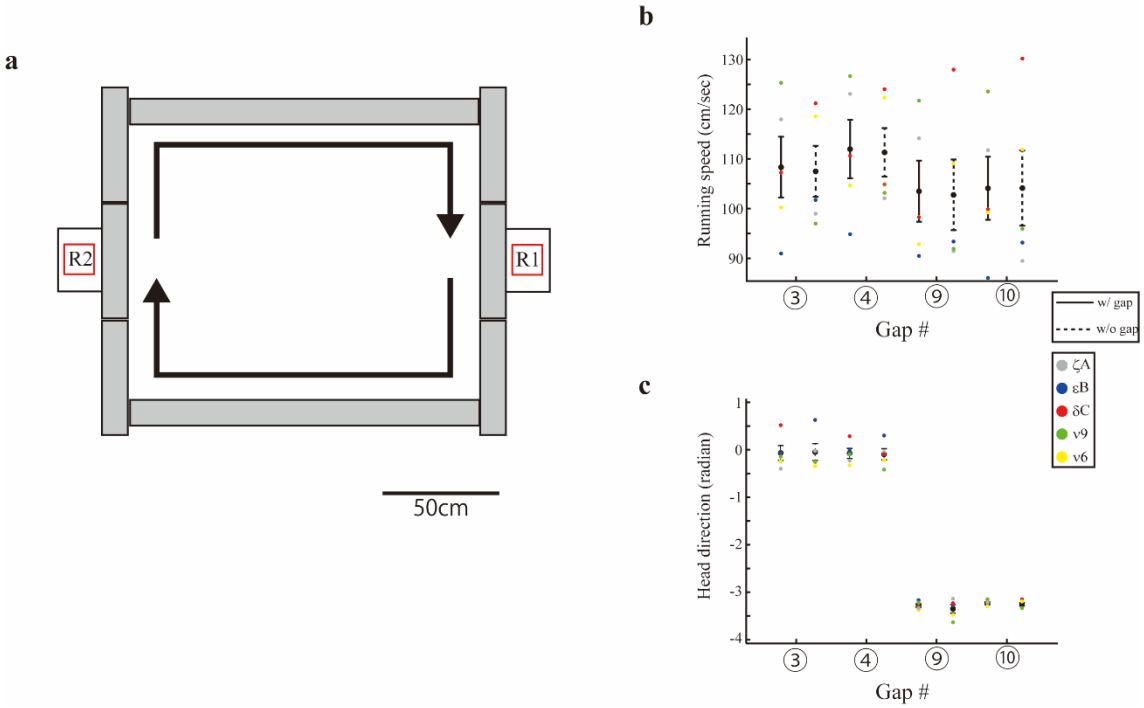

Figure S4. The running speed and head direction on the runway with or without gaps, Related to Figure 2. (**a**) Schematic showing two gapless runways placed at the top and bottom of the square-shaped maze. R1 and R2 indicate food dispensers. (**b–c**) The running speed (**b**) and head direction (**c**) of five rats on the runways with gaps (solid line) and without gaps (dotted line) as a function of the examined gap locations. The data from individual animals are overlapped as color-coded dots. Neither running speed nor head direction were influenced by the presence of a gap (simple main effect: gap presence vs. running speed between all pairs of the examined gaps: $P > 0.05$, gap presence vs. head direction between all pairs of the examined gaps: $P > 0.05$). However, there were interactions between gap presence and location (running speed: $F_{1,4} = 2653.9$, $P < 10^{-6}$; head direction: $F_{1,4} = 302.3$, $P < 10^{-4}$) shown using two-way repeated-measures ANOVA. Error bars indicate SEM.

Table S1. Dimensions of the runway for the rat version of the reconfigurable maze, Related to Figure 1.

Runway type	Combination			
Straight	A, B, C, D, E			
Right	C, F, G, H, I, J, K, L, T			
Left	C, F, G, H, I, J, K, L, T			
Central	C, F, H, I, J, K, L, T			
S-shaped	H, M, N, O, P			
Right and Left	C, Q, R, S, T			
Octagonal field	W, X, T			
Long straight	C, U, V, T			
Basic component	Polygon type	Depth (mm)	Width (mm)	Height (mm)
A	Rectangle	5	490	100
B	Rectangle	5	490	45
C	Rectangle	2	100	5
D	Rectangle	5	100	5
E	Rectangle	5	440	10
F	Non-regular	5	485	100
G	Rectangle	5	485	45
H	Rectangle	5	100	45
I	Rectangle	5	260	45
J	Rectangle	10	480	15
K	Non-regular	10	480	15
L	Non-regular	2	230	10
M	Non-regular	5	480	100
N	Rectangle	5	305	45
O	Non-regular	10	480	15
P	Non-regular	2	180	10
Q	Non-regular	5	490	100
R	Non-regular	2	330	10
S	Non-regular	10	450	15
T	Rectangle	5	100	10
U	Rectangle	5	685	100
V	Rectangle	5	100	10

		Depth (mm)	Side (mm)	
W	Octagon	5	140	
X	Non-regular	2	140	

Runways can be assembled using a combination of basic components (A-X). All 3D models are freely available (https://github.com/TakahashiLab/ReconfigurableMazeParts).

Table S2. Dimensions of the runway for the mouse version of the reconfigurable maze, Related to Figure 1.

Runway type	Combination			
Straight	A, B, C, D			
Right	A, B, C, D, G, H, I			
Left	A, B, C, D, G, H, I			
Right and Left	A, C, D, G, H, I			
Central	A, C, D, E, F			
Basic component	Polygon type	Depth (mm)	Width (mm)	Height (mm)
A	Rectangle	3	391	40
B	Rectangle	3	391	28
C	Rectangle	10	40	10
D	Rectangle	3	40	5
E	Rectangle	3	140	28
F	Rectangle	3	115	5
G	Rectangle	3	40	15
H	Rectangle	3	80	5
I	Rectangle	3	311	28

Runways can be assembled using a combination of basic components (A-I). All 3D models are freely available (https://github.com/TakahashiLab/ReconfigurableMazeParts).

Table S3. Variability between rats: electrophysiological measurements, Related to Figure 5.

RAT #	ζA	δB	δA	εA	Total
No. of pyramidal cells	89	40	46	35	210
No. of interneurons	8	4	9	5	26
Analyses for the square-shaped maze for gap effects					
No. of place cells (spatial information > 0.1 bit/spike & peak firing rate > 1 Hz)	28	18	14	2	62
Spatial information (bits/spike, mean ± sem)	0.41±0.05	0.30±0.03	0.66±0.13	0.22±0.06	
Unit isolation quality (isolation distance, Median ± QD)	8.3 ±5.5	5.9 ±12.2	14. 1 ±8.7	6.4 ±2.7	
Analyses for the maze morphing from square to cruciform to square					
No. of place cells (spatial information > 0.1 bit/spike & peak firing rate > 1 Hz in any of three situations)	60	24	28	17	129
Spatial information (bits/spike, mean ± sem)	0.67±0.11	0.24±0.03	1.06±0.17	0.96±0.34	
Unit isolation quality (isolation distance, Median ± QD)	8.3 ±5.6	6.7 ±6.2	6.9 ±8.0	6.8 ±3.6	

(*) The number of cells meeting the criteria had a large difference between the two conditions because some cells met the criteria either in the square-shaped maze or in the cruciform maze during morphing.

Supplemental Video legends

Supplemental Video 1. Morphing of a maze from square to cruciform by S.H. (expert), Related to Figure 1.

Supplemental Video 2. Morphing of a maze from square to cruciform by K.M. (expert) , Related to Figure 1.

Supplemental Video 3. Morphing of a maze from square to cruciform by R.T. (expert) , Related to Figure 1.

Supplemental Video 4. Morphing of a maze from square to cruciform by K.I. (beginner) , Related to Figure 1.

Supplemental Video 5. Morphing of a maze from square to cruciform by H.A. (beginner) , Related to Figure 1.

Supplemental Video 6. Morphing of a maze from square to cruciform by S.T. (beginner) , Related to Figure 1.

Transparent Methods

Maze system implementation. The reconfigurable maze consists of interlocking runways (49 cm × 10 cm for rats, see Table S1; 39 cm × 5 cm for mice, see Table S2) and an array of accompanying parts including feeders, movable walls, shut-off sensors, and treadmills. Each runway is placed atop a tower mounted on a breadboard with a grid of holes (hole-to-hole spacing: 25 mm for rats, 25 mm for mice), that enables each section to be mounted independently of other runway sections. For rats, each runway made of 5 mm thick black polyvinyl chloride (PVC) (matte finish) is 55 cm above the breadboard (Table S1). For mice, 3 mm thick gray PVC is 34 cm above the breadboard (Table S2). The tower and its baseplate are made of aluminum. For rats, the baseplate has four protrusions that can be inserted into the holes of the breadboard to attach it. For mice, a bolt was inserted into the holes because the weight of the baseplate was too light to support the runway. Sidewalls (45 mm height for rats; 30 mm height for mice) around the top of the runway prevent the rats and mice from slipping off the runway. The elevated runways prevent the rats and mice from jumping out of the maze. The maze sits within a shielded enclosure (4 m × 5 m for rats; 1.8 m × 3.0 m for mice) covered by a copper mesh. All metal parts are grounded to reduce electrical artifacts in the electrophysiological recording.

An Arduino Mega controller was used to receive signals from shut-off sensors and to send activation signals to the actuators in the treadmills and feeders according to the user-defined sensor and actuator schedule. Custom-made scheduling software written in Matlab was used to monitor the location of rat or mouse via shut-off sensors and to control the actuators in the treadmills and feeders, which enables the feeders to be turned on and off according to the location of rats or mice.

Animals. Ten Long–Evans rats and four C57BL/6J mice purchased from Shimizu Laboratory Supplies, Co. Ltd. (Kyoto, Japan) were housed individually in cages (20 × 25 × 23 cm for rats, 14 × 21 × 12 cm for mice) where the light was maintained on a 12-hour light/12-hour dark schedule with the light phase starting at 8:00 am. The tests were performed in the light phase. The weight of all rats or mice was kept at 80% of free-feeding body weight. To examine hippocampal place coding on the maze, a custom-made microdrive was implanted into the dorsal hippocampal CA1 of both hemispheres (eight tetrodes each) of four rats to record multiple single-unit activities. All procedures were approved by the Doshisha University Institutional Animal Care and Use Committees.

Surgery, electrode preparation, and recording. Under isoflurane anesthesia, a custom-made microdrive with 16 independently movable tetrodes was fixed to the skull above the

hippocampus of both hemispheres (eight tetrodes each; AP 3.8 mm, ML 3.0 mm, DV 0.5–1.0 mm) of four rats (Table S3). After surgery, the electrodes were individually lowered into the pyramidal cell layer of the dorsal hippocampal CA1. The extracellular signals were amplified, buffered, digitized, and continuously sampled at 25 kHz using two 32-channel RHD2000 chips (Intan Technologies, Inc., CA) via a motorized commutator (*AlphaComm-I*; AlphaOmega Inc., Israel). The spikes and local field potential (LFP) were digitally filtered at 800–7.5 kHz and 0.1–200 Hz, respectively. The occurrence of sharp-wave ripple events in the LFP during immobility periods was used to estimate the pyramidal cell layer. After spike sorting using *KlustaKwik*, putative principal cells were distinguished from fast-spiking cells based on average firing rate (5 Hz). We defined place cells if the following criteria were met: the overall firing rate was >0.1 Hz, spatial information was > 0.1 bit/spike, and maximum firing rate was >1.0 Hz.

Behavioral training. All rats and mice were food-restricted and reduced to 80% of their ad libitum body weight over a two-week period before training. During this time, they were handled daily. To train rats or mice to obtain pellets from the food dispenser, they were initially placed on a box (48 cm × 24 cm, 32 cm height for rats; 34 cm × 24 cm, 19.5 cm height for mice) with the food dispenser at a corner.

Rats. The rats were trained on L, C, or G-shaped mazes configured by the reconfigurable maze system in the testing enclosure where they were habituated to the sounds made by the movable walls being raised and lowered. The rats performed a small, square-shaped maze task (overall: 120 cm × 49 cm) in which they ran in a clockwise direction to obtain a pellet. The training lasted until the rat learned to obtain at least one pellet per minute within a 25-minute experimental period. Next, the rats trained to run in a clockwise direction in a large square-shaped maze (overall: 170 cm × 148 cm) to obtain pellets from two food dispensers located at the left and right sides of the maze. The training lasted for at least 25 minutes per day and continued until the criteria of at least one trial per minute was achieved over one week. After the initial training, rats were trained to perform in the morphing experiment and the spatial alternation tasks described below.

Mice. Unlike the rats, the mice were trained on a linear track with a movable wall where they obtained food pellets at both sides and were habituated to the sounds of the movable wall. The mice performed a rectangle-shaped maze task (overall: 49 cm × 80 cm). The training lasted until they learned to obtain at least one pellet per minute for 25-minute intervals. After the initial training, they were trained to run on the figure-8 shaped maze, double T-maze, plus maze, and W-maze to obtain food pellets.

Morphing experiment. Four rats were trained to run in a clockwise direction on the maze morphing from square to cruciform to square. They ran within ~1 hour in the following sequence:

square maze, cruciform maze, and square maze. The 15-minute long sequences were spaced at ~5-minute intervals, and the rats were rewarded each time they arrived at the food dispensers located at both the left and right sides of the maze. Each maze morphing was done within approximately 5 minutes. The unit recording was made after the rats had experienced the maze morphing over a few days.

Spatial alternation task.

Rats. Five rats were trained to alternate between left and right at a decision point on the figure-8 shaped maze until they achieved an 85% correct rating for 25 minutes. A delay period was then incorporated. During the delay period, rats were locked between two movable walls in front and behind a treadmill. The treadmill rotated at a constant speed (~20 m/min) during the delay period. The delay period was incremented from 1 sec to 7 sec every testing day.

Mice. Three mice were trained to alternate left and right at two decision points on the double T maze until they achieved a 75% correct rating for an hour (Figure 4g).

Animal trajectory and head direction. The tip and root of the head were tracked from images captured at 50 or 100 frames per second by a USB3.0 digital video camera mounted on the ceiling of the enclosure using *DeepLabCut* (Mathis *et al.*, 2018). Initially, 200 annotated images were used to train the pre-trained ResNet-50 network using transfer learning. A few additional iterations of training were then performed with the goal that all Euclidian distances between tracked locations in adjacent frames would be under 50 pixels. Running trajectory was reconstructed by concatenating the tracked root of the head. Head direction was computed from the tip and root of the head by the inverse of the tangent function.

Analyses. The rat's trajectory was linearized for each trial by projecting the actual trajectory onto a predefined idealized trajectory using nearest-neighbor Delaunay triangulation. Spatial bins had a resolution of approximately 3 cm.

Rate map. A firing rate map of well-isolated neurons was constructed in a standard manner by dividing the total number of spikes in a bin (3 cm × 3 cm) at a given location by the total amount of time that the rat has been in that bin. Each value was smoothed with a Gaussian filter with a variance of three.

MUA. MUA was calculated by summing the firing of all monitored cells including low-firing cells and fast-spiking cells.

Spatial information. The spatial information (bits per spike) was used to measure how much information a spike conveys about the rat's location on the maze (Skaggs *et al.*, 1993). This is calculated by the following formula:

$$Spatial\ information = \sum_i P_i \left(\frac{R_i}{R}\right) \log_2 \left(\frac{R_i}{R}\right)$$

where *i* indexes over the position bins, P_i is the probability that the rat was in bin *i*, R_i is the mean firing rate in bin *i*, and *R* is the overall mean firing rate. On the basis of the spatial information, we identified the place cells.

Spatial and rate similarity measures. The spatial similarity is expressed by calculating the spatial correlation of place fields between the spatially overlapping paths of the square and cruciform mazes. The difference in firing rates was expressed by calculating a difference/sum score (Leutgeb *et al.*, 2005). The unsigned difference between the two maximum firing frequencies was calculated, and the difference was divided by the sum of the two rates to obtain the score for a set of conditions during maze morphing. Both similarities were also expressed using the cumulative distribution function, f (X < x), which gives the probability that the variable X will be X < x for each real number x.

Bayesian decoding. A memoryless Bayesian decoder (Zhang *et al.*, 1998) was used to decode the rat's locations on the basis of place cell activity. First, the probability of an rat's location given place cell firings within a time window was estimated as follows:

$$\mathrm{Prob}(Pos \mid spikes) = \left(\prod_{i=1}^{N} f_i(Pos)^{n_i}\right) \quad \exp^{-\tau \sum_{i=1}^{N} f_i(Pos)}$$

where f_i and n_i represent the place map and the number of spikes of the *i*-th place cell within the time window, respectively, N indicates the total number of place cells, and τ represents the duration of the time window.

The probability within each time window was normalized for every location as follows(Pfeiffer and Foster, 2013):

$$\mathrm{nProb}(Pos \mid spikes) = \mathrm{Prob}(Pos_k \mid spikes) \Big/ \sum_{k=1}^{M} \mathrm{Prob}(Pos_k \mid spikes)$$

where Prob(Pos_k | *spikes*) represents the probability at the *k*th location bin within the time window, and M represents the total number of location bins.

The time window was set at 300 ms. A point estimation of the location was made using the maximum likelihood estimation.

Statistical analyses.

Analyses of rat's behavior around the gaps. Any value of running speed or head direction that exceeded more than three times the local scaled median absolute deviations (MAD) away from the local median within a sliding window (~72 cm) was defined as an outlier. The two-tailed

Wilcoxon rank-sum test was used to assess the gap effect on rat's behaviors in terms of running speed and head direction (Fig. 2b–c). Differences in running speed and head direction between gap locations between runways and the corresponding locations on the long gapless runway were assessed by two-way repeated-measures ANOVA (Fig. S4b–c). Differences in occupancy time at gap locations were assessed by one-way repeated-measures ANOVA (Fig. 2d). The occupancy time was calculated as the duration when the rat occupied the gap location. The duration while the rat paused (running speed < 5 cm/s) was excluded from the analysis.

Analyses of neural activity around the gaps. To examine whether the width of the place field was specifically changed at the gap locations, the Monte Carlo method was used. For each cell, the original place field location was shifted by a pseudo-random interval between 20 bins and 20 bins less than the length of the entire linearized track, with the end of the track wrapped to the beginning. This procedure was repeated 3,000 times for each cell. For each shuffling, the width of place field that is defined as the length of the firing field whose firing rate is over one-third of its maximum firing rate was calculated. Whether the place field on the gaps had a width greater than the 5^{th} percentile or lower than the 95^{th} percentile of the shuffled data was examined (Fig. 3b). Two-tailed Wilcoxon rank-sum test was used to assess the number of place fields, firing rates of MUA, and Bayesian decoding errors on the gap locations as compared with those on the non-gap locations (Fig. 3c-d, f).

Analyses of learning performance. The differences in learning curves were assessed using one-way repeated-measures ANOVA (Fig. 4). Two-way mixed ANOVA was used to ascertain the effect of expertise and experience on assembly time, and their potential interaction (Fig. 1j-k). The difference in spatial and rate similarities was assessed using the two-tailed Wilcoxon signed-rank test (Fig. 5c–d).

Analysis software. All analyses were performed using custom-made programs based on Matlab functions (v9.6; MathWorks, Natick, MA).

Histology. To identify the final recording locations, four rats were deeply anesthetized with isoflurane (Pfizer Japan Inc., Tokyo, Japan) and then given an overdose of pentobarbital sodium salt (50mg/kg, intraperitoneal (i.p.); Nacalai Tesque Inc., Kyoto, Japan) and transcardially perfused with phosphate-buffered saline (PBS), followed by 10% phosphate buffered formalin fixative (3.5-3.8% formaldehyde). Their brains were cut coronally at 40 μm and stained with cresyl violet. The final location of the tip of each electrode was around or below the pyramidal cell layer of the dorsal hippocampal CA1.

Supplemental References

Leutgeb, S. *et al.* (2005) ‘Independent codes for spatial and episodic memory in hippocampal neuronal ensembles.’, *Science*, 309(July), pp. 619–623. doi: 10.1126/science.1114037.

Mathis, A. *et al.* (2018) ‘DeepLabCut: markerless pose estimation of user-defined body parts with deep learning’, *Nature Neuroscience*, 21(9), pp. 1281–1289. doi: 10.1038/s41593-018-0209-y.

Pfeiffer, B. E. and Foster, D. J. (2013) ‘Hippocampal place-cell sequences depict future paths to remembered goals.’, *Nature*, 497, pp. 74–9. doi: 10.1038/nature12112.

Skaggs, W. E. *et al.* (1993) ‘An information-theoretic approach to deciphering the hippocampal code’, *Advances in neural information processing systems*. Edited by S. J. Hanson, J. D. Cowan, and C. L. Giles, 5(2), pp. 1031–1037.

Zhang, K. *et al.* (1998) ‘Interpreting neuronal population activity by reconstruction: unified framework with application to hippocampal place cells.’, *Journal of neurophysiology*, 79, pp. 1017–1044.